Crisis in the periodic Lorentz gas

C. P. Dettmann[*] and G. P. Morriss

School of Physics, University of New South Wales, Sydney 2052, Australia
(Received 14 June 1996; revised manuscript received 14 August 1996)

The attractor of the nonequilibrium Lorentz gas covers the whole of the accessible phase space at small values of the field. Here we investigate the transition from this state to a state with fractal support, corresponding to a discontinuity in the box dimension as a function of field. A number of numerical techniques are employed, the most effective involving symbolic dynamics. It is found that above the transition, the dynamics is effectively irreversible in a manner not evident below the transition. A similar crisis occurs at different spacings and rotation angles. [S1063-651X(96)10111-2]

PACS number(s): 05.45.+b, 05.70.Ln

I. INTRODUCTION

Certain nonequilibrium systems have the odd property, noted by Hoover and Moran [1], that although the dynamics is dissipative, leading to phase-space contraction on the average and multifractal attractors [1,2], these attractors fill the available phase space and thus have a box dimension equal to that of phase space. The most well understood such system is the nonequilibrium periodic Lorentz gas [3–5] in two dimensions, for which a number of rigorous results may be proved [6] for sufficiently small field. At this point it is natural to ask at what value of field the attractor ceases to be space filling and what the nature of this transition is. Here we attempt to answer these questions, and find that the behavior is quite subtle and is related to a breakdown of one form of reversibility.

The Lorentz gas is the simplest of a number of nonequilibrium molecular-dynamics (NEMD) models that are used to relate the macroscopic properties of nonequilibrium steady states, such as transport coefficients, to microscopic dynamics [7]. The Lorentz gas is a classical model of electrical conduction and it shares many of the features of more elaborate models. We discuss other NEMD models in Sec. VI. We consider a particle colliding with a periodic hexagonal array of hard disks of radius 1. The distance between the centers is $2+w$. See Fig. 1. A common spacing is $w=0.236$, which we will use until Sec. V, where different w are considered.

Between collisions, the particle is driven by a constant external force $\mathbf{F}$ together with a Gaussian thermostat [7], which ensures that the energy of the particle is constant, set to 1/2. The presence of a thermostat in the equations permits the system to reach a steady state, despite the continual input of energy from the driving force. Other methods of simulating the loss of heat from the system all involve boundaries [8] and thus are inhomogeneous. The thermostated equations of motion are

$$\dot{\mathbf{x}} = \mathbf{v}, \tag{1}$$

$$\dot{\mathbf{v}} = \mathbf{F} - \frac{\mathbf{F} \cdot \mathbf{v}}{\mathbf{v} \cdot \mathbf{v}} \mathbf{v}, \tag{2}$$

with the solution

$$t = t_0 + \frac{1}{\epsilon} \ln \frac{\tan \theta/2}{\tan \theta_0/2}, \tag{3}$$

$$x = x_0 + \frac{1}{\epsilon} \ln \frac{\sin \theta}{\sin \theta_0}, \tag{4}$$

$$y = y_0 + \frac{\theta - \theta_0}{\epsilon}, \tag{5}$$

$$\mathbf{v} = \cos \theta \hat{\mathbf{x}} + \sin \theta \hat{\mathbf{y}}. \tag{6}$$

Here a subscript zero indicates the initial value $\mathbf{F} = -\epsilon \hat{\mathbf{x}}$, and the sign of θ is determined by the initial value and does not change during a free flight. The angle between the field and a line of scatterers ϑ is another parameter, which is usually set to zero. We consider nonzero values of ϑ in Sec. V. Note that Hoover and Moran [1] use a field of "$3P^2/m\sigma$," which corresponds to a field of $\epsilon = 1.5$ in our units, and also use $\vartheta = \pi/6$, unlike most other authors.

These equations are time reversible, so that any trajectory remains a trajectory with the time and velocity reversed.
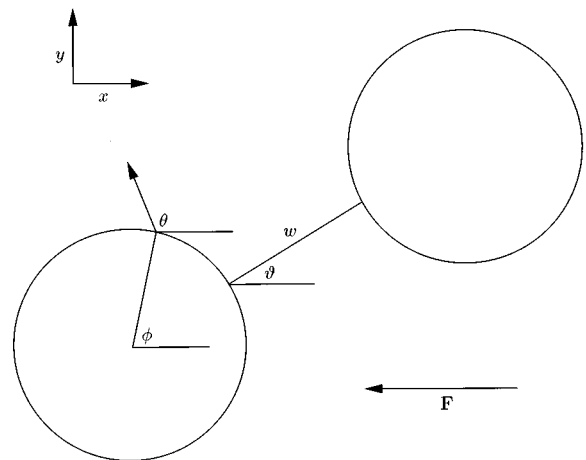
FIG. 1. Geometry of the Lorentz gas. For most of this paper we use $w=0.236$ and $\vartheta=0$.

[*] Electronic address: c.dettmann@unsw.edu.au

<u>54</u>   4782

Nevertheless, almost all (relative to the Liouville measure) initial conditions lead to motion along the field at an average rate defined by the current

$$\mathbf{J} = \lim_{t \to \infty} \frac{\Delta \mathbf{x}}{t}. \qquad (7)$$

Depending on ϑ, $\mathbf{J}$ may not be parallel to $\mathbf{F}$ [5], but $\mathbf{J} \cdot \mathbf{F}$ is always positive (except in elliptic regions, below, where it is zero) and gives the rate of dissipation of energy in the system. This is the usual sense in which these systems are understood to be irreversible. A periodic orbit description may be found in Ref. [9]. We can say that the system is microscopically reversible (due to the equations of motion), but macroscopically irreversible (due to the sign of the current). We will introduce another form of irreversibility in Sec. III.

The Lorentz gas at large values of field has been studied by Lloyd *et al.* [10], who found several different types of behavior, including a breakdown of ergodicity, integrable elliptic regions, and stable orbits. Here, as in Ref. [10], ergodicity is defined as the property that almost all initial conditions lead to the same attracting measure; other authors also require the attractor to be space filling. Thus there are different classes of chaotic crisis, depending on the features of the dynamics on either side of the transition. The crisis investigated in most of this paper occurs for all values of the spacing (but see Sec. V) and lies between the space-filling region at low field and an ergodic but non-space-filling region at higher fields, which was not explicitly mentioned in Ref. [10].

II. GENERALIZED DIMENSIONS

There is often confusion about the precise meaning of various terms in the chaos literature, so we begin with a few definitions. Any absolutely continuous distribution (with respect to Liouville measure) that is evolved forward (backward) in time approaches a stationary distribution, which will be termed the *attractor* (*repeller*) [6]. The generalized (Renyi) dimension D_q of a distribution is defined by [11]

$$D_q = \frac{1}{q-1} \lim_{\varepsilon \to 0} \frac{\ln \sum_i p_i^q}{\ln \varepsilon}. \qquad (8)$$

Here p_i is the measure contained in the cells of a grid of size ε. For $q \leq 0$ only nonzero p_i are included. For $q = 1$ the limit is taken on the above expression to obtain

$$D_1 = \lim_{\varepsilon \to 0} \frac{\sum_i p_i \ln p_i}{\ln \varepsilon}. \qquad (9)$$

The most commonly used dimensions are D_0, called the capacity or box counting or (inaccurately [12]) the Hausdorff dimension, D_1 the information dimension, and D_2 the correlation dimension. There are several equivalent ways to define the sum in Eq. (8), such as covering the distribution with disks of radius ε (see Ref. [12]). D_0 gives the dimension of the support of a measure, independent of how it is distrib-

uted. D_1 gives the scaling of information required to locate a point in the distribution with length and equally weights parts of the distribution proportional to the measure contained in them (see Sec. IV). D_2 gives the scaling of the two point correlation function and similarly for higher integer q. $D_{q_1} \geq D_{q_2}$ if and only if $q_1 \geq q_2$ with equality if the distribution is uniform [11].

The generalized dimensions may be calculated using Eq. (8) by fitting a straight line to a log-log graph, but this requires a large number of data points, particularly for $q < 0.5$. Larger values of q are not such a problem, as the peaks of the distribution dominate in the sum and also have the best statistical accuracy. For still larger values, say $q > 3$, the limiting factor is the grid size, as the total number of contributing grid points becomes very small, leading to greater uncertainty. We evaluate D_q in this paper to a reasonable degree of accuracy by counting an average of 8000 points per grid square, but other, more definite measures will be used to identify the transition from space-filling to non-space-filling attractors in Sec. III.

For the special values of $q = 1$ and $q = 2$ there are much faster algorithms for finding the dimension of an attractor using the correlation function [11]. In addition, for our system, the Kaplan-Yorke relation

$$D_1 = D_{\mathrm{KY}} \equiv 1 + \frac{\lambda_1}{|\lambda_2|} \qquad (10)$$

between D_1 and the Lyapunov exponents λ_i holds when $\lambda_1 > 0$ [6] and may be used to evaluate D_1 more accurately than using the above box counting method. We have also verified it numerically for a number of fields (Sec. III).

Note also that it is possible to formulate an alternative description in terms of the singularity spectrum $f(\alpha)$, which gives a measure of the distribution of points of singularity strength α. See Ref. [12] or most other texts on fractals. $f(\alpha)$ may be obtained implicitly from D_q using the relations

$$\alpha(q) = \frac{d}{dq} [(q-1)D_q], \qquad (11)$$

$$f(q) = q\alpha(q) - (q-1)D_q \qquad (12)$$

and eliminating q. As we have already noted, it is difficult to evaluate the dimensions for $q < 0$ numerically and this corresponds to $\alpha > \alpha(0)$. However, at $q = 0$ it is readily seen from the above equations that $f(\alpha)$ is a maximum and is equal to D_0. Thus a transition involving D_0 will manifest itself clearly in the $f(\alpha)$ spectrum. Since this information is equivalent to D_q, we will restrict our investigations to the latter.

It is convenient to operate in the reduced phase space consisting of the angles θ and ϕ after a collision (see Fig. 1). In this two-dimensional phase space, the dynamics is an invertible and piecewise smooth mapping. Dimensions of distributions in the full (x, y, θ) space are simply one more than in the (ϕ, θ) space. The allowed phase space consists of the values of ϕ and θ for which the particle is moving outward, that is,
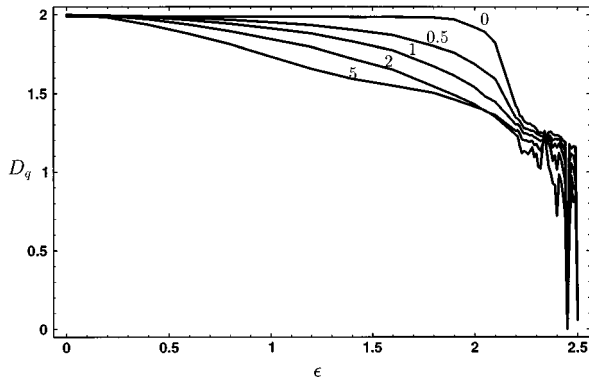
FIG. 2. Generalized dimensions as a function of field. The different curves correspond to different q.

$$|\phi - \theta| \leqslant \frac{\pi}{2} \quad (\mathrm{mod}\,2\pi). \tag{13}$$

We have numerically simulated 10^9 collisions for values of field up to 2.2 and performed the box counting algorithm described above to estimate D_q using grid sizes of up to 512^2. For fields above 2.2 the box dimension of the attractor is smaller than 2, so a smaller number of collisions (1.6×10^7) was necessary to obtain reliable values of the dimensions (differing by less than 0.01 from a couple of test cases using the larger number of collisions). The results are shown in Fig. 2. It is clear that D_0 remains very close to 2 for fields up to about 2.1 before dropping rapidly. The dimensions at large values of q decrease at a much more gradual rate. It looks quite likely from these data that D_0 is exactly equal to 2 for small but finite values of the field, but the nature of the transition to smaller values is not clear because it is difficult to get accurate results for D_0 as mentioned above.

We gain a more detailed understanding of the nature of the attractor by looking at it as a density plot in Fig. 3, which shows the attractor and repeller for fields of 2.1, 2.2, and 2.3. The repeller is obtained by considering the time-reversed motion, which in this case is a simple transformation of the attractor. In the case of $\epsilon = 2.1$, the attractor and repeller are well on the way to filling up the entire phase space, while for $\epsilon = 2.3$ they are each fractals that are disjoint. The case $\epsilon = 2.2$ appears to be an intermediate situation, with only partial overlap. Note the faint extensions of the main parts of the attractor and repeller.

We can understand this in the following manner. It is clear that the attractor is smooth in the unstable direction at a point in phase space and varies rapidly in a fractal manner in the stable direction. The repeller does the opposite. Now, if the attractor and repeller contain a common point, then they must also both contain all the iterates of that point since they are both invariant measures. All but a set of zero (attractor) measure points on the attractor have iterates that are dense on the attractor, so if the common point is one such point, the repeller will be dense on the attractor and vice versa. In this case, both sets will be continuous in both the stable and unstable directions and so will be dense in phase space. This is not a proof since it depends on the overlap being at "generic" points. However, it does provide a picture that seems to apply in our situation.

As the field is decreased from 2.3 to 2.1, it can be seen that the attractor and repeller approach one another, beginning to overlap along the line $\phi = \theta$ just above $\epsilon = 2.2$. At the crisis point the overlap is a single periodic orbit of length 2, designated (2 8) by the symbolic dynamics of Sec. III, together with a symmetry related orbit, with symbolic dynamics (4 10). As the field is decreased further, the attractor and repeller "leak out" into the surrounding phase space. At $\epsilon = 2.1$ it is clear that both fill the entire space. The amount of attractor measure outside the original region of the attractor increases with decreasing field. These considerations imply that D_0 is exactly 2 below the transition and drops discontinuously to a value between 1 and 2 above the transition. According to the classification of chaotic transitions in Chap. 8 of Ref. [13], it would appear to fit the general description of crisis induced intermittency, but the dramatic difference in the nature of the attractor above and below the critical field indicates that a more detailed description is desirable.

III. DYNAMIC PROPERTIES AND ORDER PARAMETERS

It is difficult to make definite statements about the nature of the crisis from calculations of D_0, where, as we have seen, there are large uncertainties in the results. The phase-space plots from which the dimension estimates were generated convey more information, but they are still only static invariants of the dynamics and contain no information as to which parts of the attractor map to which other parts and so on. In this section we investigate several dynamic quantities around the transition point, which lead to a deeper understanding of the nature of the crisis and also a more precise estimate of the transition point.

One example is the Lyapunov spectrum [13], which is related to D_1 by Eq. (10). The Lyapunov exponents are calculated by considering the evolution of small but finite (10^{-7}) perturbations of the trajectory from one collision to the next, followed by a Gram-Schmidt reorthonormalization. The results (Fig. 4) converge with three place accuracy reasonably quickly, showing that the fluctuations shown in the figure are real, suggesting a continuous but nondifferentiable behavior as a function of field for all values of field in the range (2.1,2.3), with no obvious features corresponding to the crisis. Thus Lyapunov exponents do not appear to be good indicators of the transition point. These results show that D_1 is also continuous over the transition, via the Kaplan-Yorke relation (10), which we have also confirmed numerically (Table I). The small discrepancies are mostly due to the use of a finite size grid when evaluating D_1.

Another powerful tool for analyzing chaotic systems is symbolic dynamics. Phase space is partitioned into disjoint subsets, each of which is given a "symbol." A trajectory can thus be represented as an infinite symbol sequence, perhaps nonuniquely. For the Lorentz gas, the obvious partition (Fig. 5) is the one that determines with which disk the particle will collide next.

At zero field, the available symbols are $0-11$, but out of the 144 possible pairs of such symbols, only 96 actually occur: the symbolic dynamics is "pruned." As the field is increased, other symbols become available and some information about the dynamics can be obtained by measuring the relative frequencies of various symbols or short sequences.
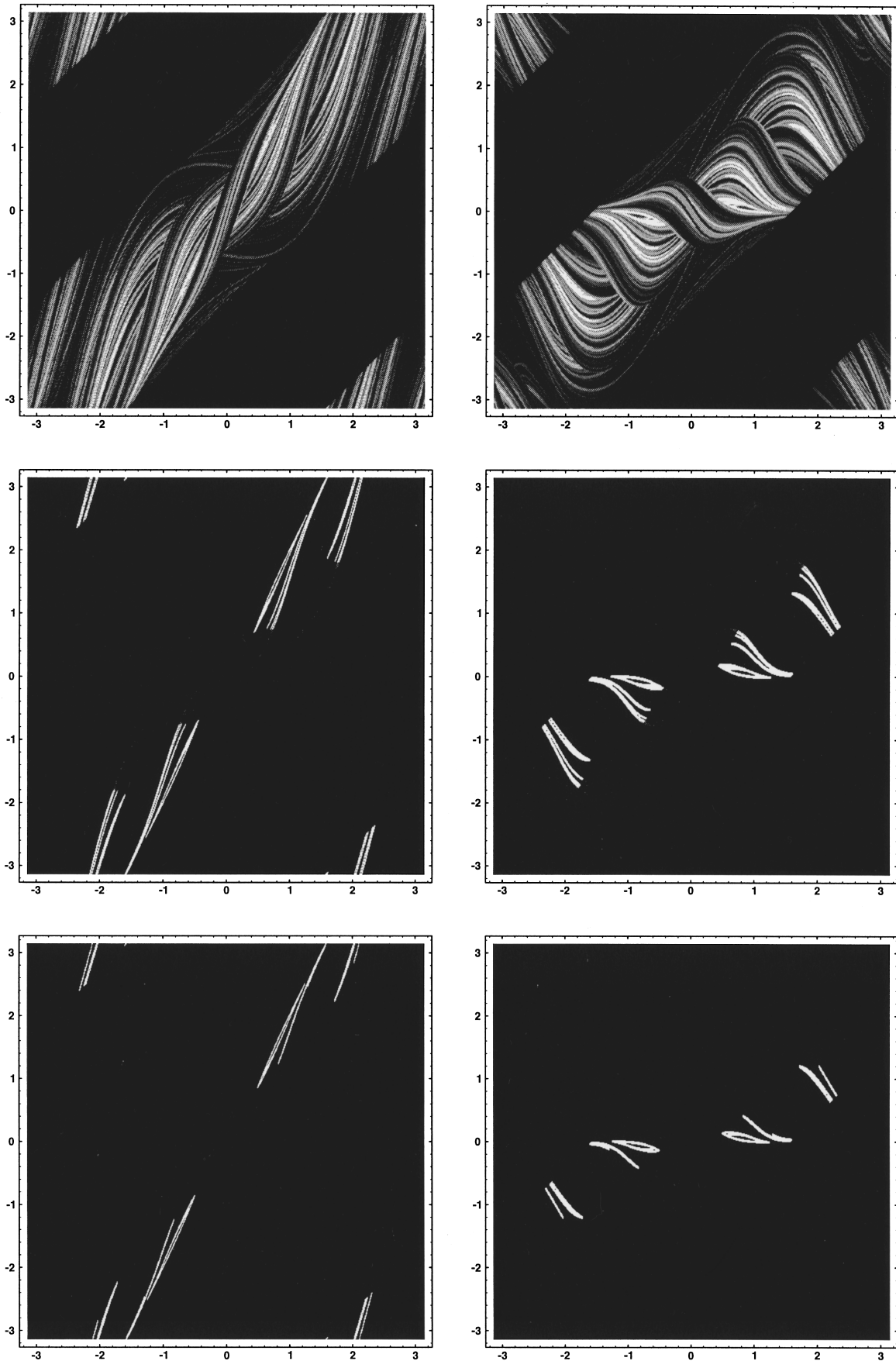
FIG. 3. Phase-space plots of the attractor (left) and repeller (right) for fields of 2.1 (top), 2.2 (middle), and 2.3 (bottom). White corresponds to a large amount of measure and black to little or no measure, with a logarithmic gray scale in between. The horizontal axis in each plot is ϕ and the vertical axis is θ.
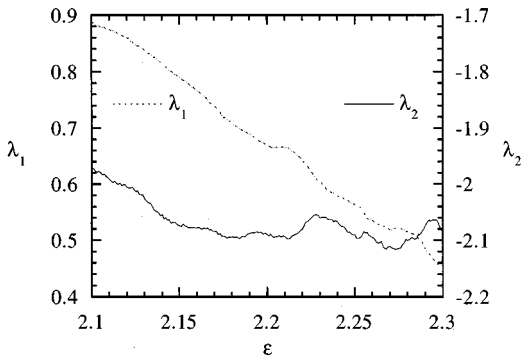
FIG. 4. Lyapunov exponents as a function of field.

FIG. 5. Symbolic dynamics for the Lorentz gas. The symbol is a number determined by the relative separation of one disk and the next, using the central disk above as a reference point. For example, the symbol 0 corresponds to a translation of one lattice vector in the x direction, opposite the field.

Below the transition, the available symbols appear to be $\{0-2,4-8,10,11,18\}$, with 1, 11, and 18 quite rare. As the field is increased from 2.1 to just above 2.2, the frequencies of these, and also 0, 5, and 7 decrease to zero, leaving just $\{2,4,6,8,10\}$. The pairs of symbols that are seen to occur above 2.2 are $\{2\rightarrow6,2\rightarrow8,4\rightarrow8,4\rightarrow10,6\rightarrow2,6\rightarrow4,6\rightarrow8, 6\rightarrow10,8\rightarrow2,8\rightarrow4,10\rightarrow4,10\rightarrow6\}$, with $6\rightarrow2$ and $6\rightarrow4$ always preceded by 10 and $6\rightarrow8$ and $6\rightarrow10$ always preceded by 2. From this we can see that, given a particular symbol sequence, there are at most two possibilities for the next symbol, so it is possible to relabel the symbolic dynamics in terms of only two symbols. From Fig. 5 it can be seen that these two choices do not permit more than one trajectory segment in a row to be against the general direction of the field. The overall motion of the particle is along a channel formed by the disks, in the direction of the field.

The transition from a space-filling to a fractal attractor has thus broken one form of reversibility: Below the transition a generic (i.e., with initial conditions chosen with respect to the Liouville measure) trajectory will fill phase space with a multifractal distribution defined by the attractor. On the average, there is a general drift in the direction of the field at a rate given by the current $\mathbf{J}$; however, on rare occasions the particle moves against the field for a short time. Because the equations of motion are reversible and the trajectory fills up phase space, the particle moves an arbitrary distance against the field, but with a frequency that is inversely proportional to the exponential of the distance. Above the transition, however, a generic trajectory as defined above has some transient behavior after which it never has more than one collision opposite the field in a row. In a very real sense the behavior is irreversible on small scales as well as large ones, discounting the set of zero (Liouville) measure initial conditions that lead to, for example, the time reversal of generic trajectories. We term this *mesoscopic irreversibility*. In terms of the concepts used in Sec. II, the attractor and repeller have become disjoint, so once a trajectory is close to the attractor, it never moves close to the repeller.

TABLE I. Confirmation of the Kaplan-Yorke relation (10) near the transition.

Field	2.1	2.15	2.2	2.25	2.3
D_1	1.45	1.37	1.30	1.25	1.22
D_{KY}	1.451	1.381	1.321	1.270	1.221
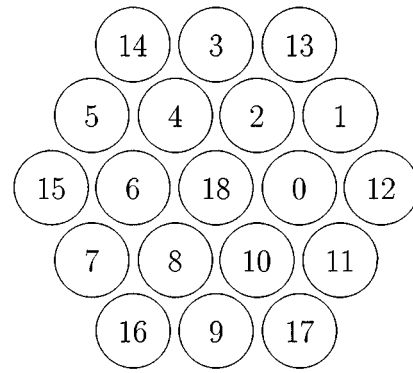
Also, because the motion is along a single channel in the lattice above the transition, the perpendicular (y) component of $\mathbf{J}$ is less than a lattice spacing divided by the time, while below the transition, there are fluctuations proportional to $t^{-1/2}$. The parallel component continues to fluctuate in this manner until the attractor collapses entirely, leaving stable periodic orbits. This anisotropy in the fluctuations of $\mathbf{J}$ is probably the best macroscopic indicator of the transition.

The symbolic dynamics may also be used as an ''order parameter'' to make a quantitative measure of the dynamics as the crisis is approached from below. In particular, we count the number of times each symbol occurs in a long sequence. Another order parameter is suggested by the phase space plots (Fig. 3). The attractor and repeller are related by a simple transformation about the line $\theta=\phi$, which corresponds to perpendicular collisions. Above the crisis, all collisions have $|\theta+2\pi m|>|\phi|$, if the value of the integer m is chosen so that $|\theta+2\pi m-\phi|<\pi/2$. Referring back to Fig. 1, in these collisions, the particle leaves the scatterer in a direction that is closer to the direction of the field than a perpendicular collision, except possibly if $m\neq0$ in which case the particle's direction is at least closer to the field than opposite it. We will call such a collision a ''forward'' collision and a collision that does not fit into this category a ''backward'' collision. As the crisis is approached from below, the number of backward collisions decreases to zero.

We have generated a logarithmic plot of the frequencies of both the 0 and the sum of 5 and 7 symbols, and the backward collisions as a function of field in Fig. 6. The 5 and 7 symbols are equivalent by symmetry, so they are included together. The vertical distances between the three curves, that is, the logarithm of the ratios, are constant, indicating that all of these measures of the distance from the transition are related. We will attempt to describe this mathematically in the following section. Note that the curves are by no means smooth, so that no ''critical exponents'' may be defined. The critical field is shown to be just greater than 2.2.

IV. DISTRIBUTION ANSATZ

In this section we formulate an approximate mathematical representation of the attracting measure in the vicinity of the
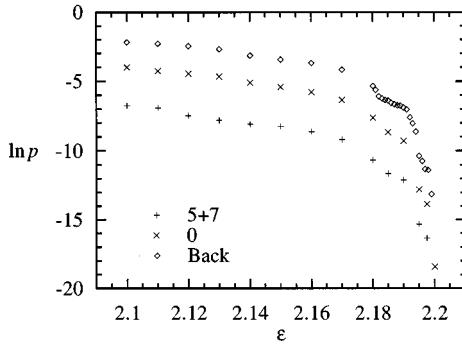
FIG. 6. Frequencies of ''backward'' collisions and the symbols 0, 5, and 7 (which are equal due to symmetry) together below the transition. Note that the ratios between the various curves are roughly constant.

crisis. This fits a number of the results we have so far into a consistent framework and permits predictions to be made concerning the behavior of D_q near the transition, which is difficult to measure directly.

The order parameters used at the end of the preceding section were all based on the amount of attracting measure in certain regions of phase space, which vary gradually with field. This suggests that, to some level of approximation, the distribution in the phase space that is not included in the attractor just above the transition is proportional to some constant distribution multiplied by a scale factor that depends on field in a manner given by Fig. 6. The rest of the distribution lies along what becomes the attractor. We can write this mathematically as

$$\mu(\epsilon) = g(\epsilon)\mu_1 + [1-g(\epsilon)]\mu_2, \tag{14}$$

where μ is the full attracting measure, μ_1 is the part that vanishes at the transition, and μ_2 is the part that remains nearly constant. All three measures are normalized to 1, and $g(\epsilon)$ is proportional to the curves in Fig. 6 and tends to zero at the transition. Of course, this relation is not intended to be exact, as both μ_1 and μ_2 are expected to change slowly in both their support and how the measure is distributed on that support as a function of field.

Equation (14) may be substituted into the generalized dimension formula (8) to obtain

$$D_q(\mu) = \frac{1}{q-1} \lim_{\varepsilon \to 0} \frac{1}{\ln\varepsilon} \ln\left[g^q \sum_i p_{1i}^q + (1-g)^q \sum_i p_{2i}^q \right]$$

$$= \lim_{\varepsilon \to 0} \frac{1}{\ln\varepsilon} \ln[c_{1q}^{1/(q-1)} g^{q/(q-1)} \varepsilon^{D_{1q}} + c_{2q}^{1/(q-1)}$$

$$\times g^{q/(q-1)} \varepsilon^{D_{2q}}], \tag{15}$$

where we have substituted

$$\sum_i p_i^q = c_q \varepsilon^{(q-1)D_q} \tag{16}$$

and c_q is of order unity. As ε is decreased, it passes a value

$$\varepsilon_c = g^{q/[\Delta D(q-1)]}, \tag{17}$$

where the two terms in the logarithm are roughly equal ($\Delta D = D_{2q} - D_{1q}$), after which the term with the largest D_q (for $q < 1$) or smallest D_q (for $q > 1$) dominates. At $q = 1$ we must use Eq. (9), and both terms contribute. The dimension of the whole measure is thus

$$D_q(\mu) = \begin{cases} \max[D_q(\mu_1), D_q(\mu_2)], & q < 1 \\ g D_q(\mu_1) + (1-g) D_q(\mu_2), & q = 1 \\ \min[D_q(\mu_1), D_q(\mu_2)] & q > 1 \end{cases} \tag{18}$$

below the transition. Unfortunately, these results may not be seen using box counting algorithms, as quite modest values of the parameters (say, $q = 0.5$, $g = 0.1$, and $\Delta D = 0.3$) can lead to very small values of ε_c (here 5×10^{-4}), which correspond to grids that are not feasible numerically either because of lack of space or because too many iterations are required to achieve acceptable statistics. Paradoxically, the best case here is very small (or very large) q.

Above the transition, $D_q(\mu) = D_q(\mu_2)$. Now we expect that the dimensions of μ_1 are larger than those of μ_2 since the latter corresponds to the highly restricted binary dynamics that we have seen already. In any case, $D_0(\mu_1) = 2$ since it covers the whole space and $D_0(\mu_2)$ is much smaller, probably around 1.4.

For $q < 1$, the maximum of the two dimensions is discontinuous at the transition, but for $q \geq 1$ the generalized dimensions are expected to be continuous, as found for $q = 1$ at the beginning of Sec. III. Thus we have reproduced the main features of Fig. 2.

One of the consequences of Eq. (14) that seems unphysical is the prediction that D_q as a function of q is discontinuous at $q = 1$ below the transition. In reality, we are considering a single attractor that has a single multifractal spectrum, albeit one that has singular properties at the crisis point, so we would expect continuity in q. The discrepancy arises because, although Eq. (14) is a good approximation for the large regions of phase space counted by the order parameters of Sec. III, it must fail on very small scales, at which all parts of the attractor appear to have the same dimensions. It may be useful here to define fractal dimensions as a function of scale. One is reminded of the fact that a fractal description of structures in physics is usually valid for only a finite range of length scales, when the limitations of atomic structure, quantum mechanics, and so on are taken into account.

V. DEPENDENCE ON SPACING AND FIELD DIRECTION

In the first part of this paper we have described the transition from a space-filling to a non-space-filling attractor for a particular state point in the Lorentz gas, $w = 0.236$ and $\vartheta = 0$. Now we generalize the results to other state points.

We may use an algorithm based on backward collisions (see Sec. III) to find the crisis field as a function of spacing w. The results are shown in Fig. 7 as the curve marked D_0. Unlike many of the functions associated with this chaotic system, it appears to be smooth. For small spacings, that is, $w < 0.15$, the transition can be found for some initial conditions and not others, and an analysis of bifurcation diagrams indicates that this is due to large elliptic regions in phase space, which contain backward collisions. Initial conditions
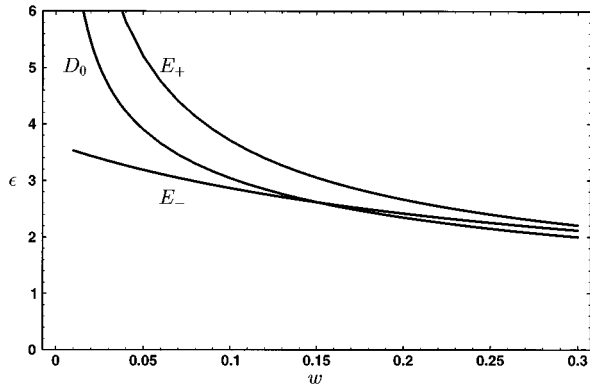
FIG. 7. Partial phase diagram for the Lorentz gas. The curve marked D_0 shows the transition from space-filling to non-space-filling attractors, at which the box dimension is discontinuous. The curves marked E_+ and E_- show the range of fields for which elliptic regions are known to occur.

of $\theta = \phi = 1.0$ appear to avoid the elliptic regions in most cases.

There is thus another way in which the attractor can cease to fill the whole of phase space: the dynamics can cease to be hyperbolic. The elliptic region and its relation to the marginally stable branch of the (4 10) periodic orbit (and the symmetry related (2 8) orbit) is described in Ref. [10]. The lowest field at which it occurs is determined by a glancing collision with another sphere, turning (4 10) into (2 6 10), which is unstable, and the highest field is determined by the disappearance of the (4 10) orbit. Both of these fields may be readily evaluated numerically, leading to the other two curves in Fig. 7.

For spacings greater than 0.15, such as 0.236, which we have been discussing, the transition from space filling to fractal occurs at a lower field than the emergence of the elliptic region and so the only effect of the latter transition is that some of the trajectories do not end up on the fractal attractor. However, for spacings less than 0.15, there is a region in field at which phase space is divided into a space-filling attractor and elliptic regions surrounding the (2 8) and (4 10) orbits. An example of this is shown in Fig. 8. Then, at some higher field, what remains of the attractor undergoes the space-filling–fractal transition we discussed previously. At fields that are higher still, there is a complicated set of crises, leading to a combination of stable orbits and chaotic attractors, reducing finally to a few stable orbits, as described in Ref. [5]. It is clearly impractical to show this in detail in Fig. 7.

Now we turn to our final investigation of the Lorentz gas: the effect of rotating the lattice so that $\vartheta \neq 0$. In particular, we choose $\vartheta = \pi/6$ (as do Hoover and co-workers [1,3]) and $w = 0.236$ as before. The ''channels'' through the lattice have now disappeared, so that the dynamics at large fields is quite different. In particular, a much larger field is required before stable orbits appear. Symbolic dynamics remains a useful tool in this situation, using Fig. 5 as before, but rotated by an angle $\pi/6$ in a counterclockwise direction, so that the field direction is now 5. The hallmark of mesoscopic irreversibility as described in Sec. III is the presence of symbols in the symbolic dynamics for which the reverses do not appear, or
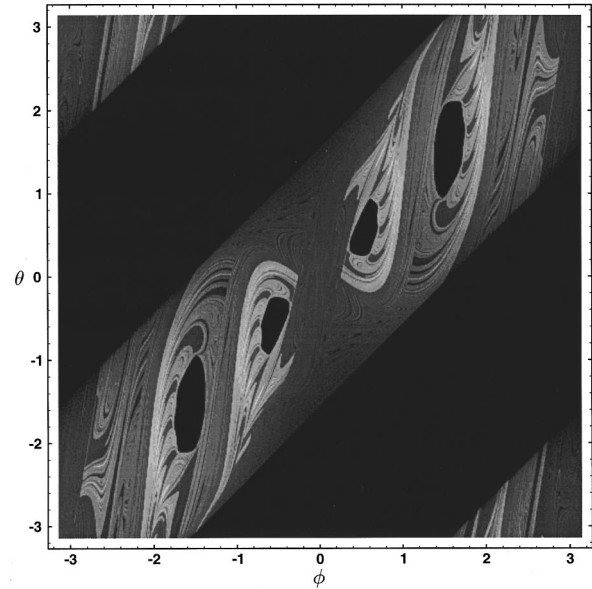
FIG. 8. Phase-space plot at $\epsilon = 3.5$ and $w = 0.05$, showing the elliptical regions, which are not reached from the given initial condition.

periodicity, showing that the attractor is a stable periodic orbit.

From the limited amount of information available in a bifurcation diagram (Fig. 9) it appears that there are two possible behaviors for this system: space-filling attractors and stable periodic orbits. We focus our attention on the first major transition from one to the other, occurring just above a field of 2.95. It is difficult to be locate the first such transition, since there may be very narrow stable windows not shown in Fig. 9. A study of the symbolic dynamics and Lyapunov exponents near the transition reveals the following.
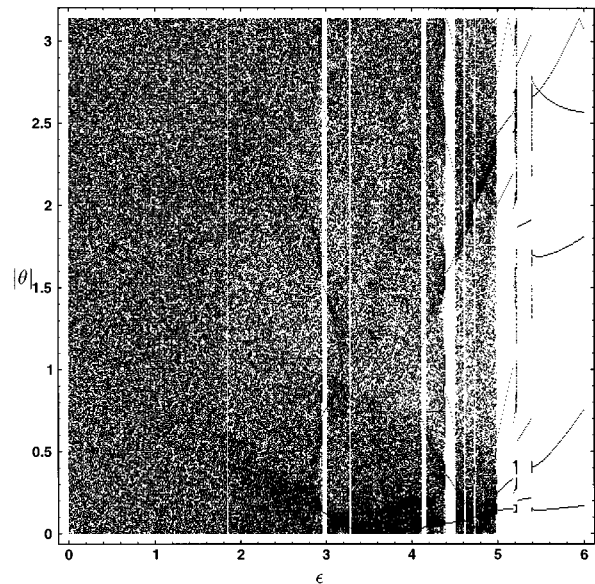
FIG. 9. Bifurcation diagram for the rotated Lorentz gas at $w = 0.236$, obtained by mapping a θ projection of the attractor as a function of field.
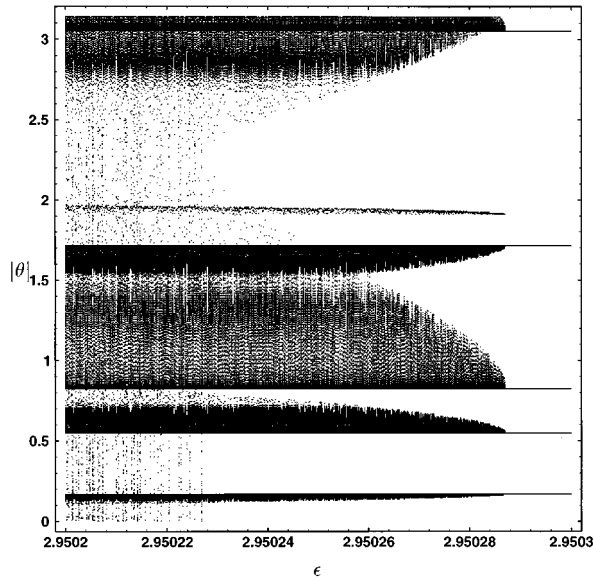
FIG. 10. Close up of Fig. 9. Note that above a field of 2.950 23, the attractor does not reach large regions of phase space: it appears to do so in this figure only because of the θ projection.

(i) $\epsilon > 2.950\,29$. The symbol sequence is periodic with the repeating sequence (0 6 4 0 6 10 4 6 10 4) and a maximum Lyapunov exponent about -0.08.

(ii) $2.950\,23 < \epsilon < 2.950\,29$. The sequence is the same as the above symbol sequence (i), with the first 4 replaced by $0 \rightarrow 5$ or the last 6 replaced by $10 \rightarrow 5$ in about 0.1 of the cycles. The spacing between the 5's varies unpredictably between fixed minimum and maximum values. The maximum Lyapunov exponent is about $+0.02$ and varies with field.

(iii) $\epsilon < 2.950\,23$. The sequence has the same behavior as that of (ii), but interrupted intermittently with numerous combinations of 2, 8, 11, and 18, as well as the above symbols in different orders. Each interruption lasts approximately 30 collisions. The frequency of interruptions and the maximum Lyapunov exponent both increase with decreasing field, until there is no trace of the original periodic sequence.

It seems from this that above a field of 2.950 29 there is a stable periodic orbit of length 10 (or possibly a multiple thereof). As the field is decreased, this orbit is pruned, that is, it passes through a scatterer, leading to the extra collisions described above. The collision is not sufficient, however, to knock the particle out of the immediate basin of attraction of the pruned orbit and it is then attracted towards the orbit before being scattered again. For still lower fields the particle sometimes escapes from this immediate basin of attraction and wanders through phase space before being captured again.

TABLE II. Phases in the Lorentz gas. Abbreviations: MR, mesoscopic reversibility; SD, symbolic dynamics.

Description	MR	SD	D_0	D_q	λ_1	λ_2
space filling	yes	rich	2	<2	+	−
fractal	no	restricted	<2	<2	+	−
elliptic	yes	periodic	1	1	0	0
stable	no	periodic	0	0	−	−

The high-field region is clearly a stable orbit; the intermediate region is chaotic, but mesoscopically irreversible in the sense of Sec. III; the low-field region has all the characteristics of a space-filling attractor. This is further illustrated by a finer bifurcation diagram, Fig. 10, which illustrates the features outlined above, in particular, the extra collision that takes place just below $|\theta| = 2$. The main point to note here is that the crisis found at $\vartheta = 0$ appears to be quite generic for the Lorentz gas and appears for a wide range of spacings and orientations. In particular, it is not simply due to the presence of ''channels'' between the disks at $\vartheta = 0$.

VI. DISCUSSION

To conclude, we summarize the main points and consider the applicability and importance of these results to other nonequilibrium systems. Given a generic (relative to the Liouville measure) initial condition, there appear to be four possible long-time behaviors for the nonequilibrium Lorentz gas, summarized in Table II. The transition from space filling to fractal occurs at a critical field that depends on the spacing of the disks and leads to crisis induced intermittency below the transition and a discontinuous change in D_0 at the crisis point. Above the transition, the attractor and repeller are disjoint, leading to a lack of reversibility on intermediate scales. Below the transition, it can be useful to approximate the attractor measure as the sum of two measures, one of which disappears at the crisis point. The most effective tool for investigating the nature of the crisis appears to be symbolic dynamics.

An exhaustive answer to the question of how much of the above analysis applies to other nonequilibrium systems is beyond the scope of this paper, but a few comments may be made here. A more extensive account will be deferred to future papers.

There are a number of other NEMD models for processes such as Couette flow and heat conduction [7]. Dimension calculations for two particle Gaussian thermostatted planar Couette flow (the SLLOD algorithm) were carried out in Ref. [2]. Here the reduced phase space is three dimensional, so accruing enough data points to fill a lattice of reasonable size (192^3 in this case) is even more difficult. Nevertheless, the calculated values of D_0 did not decrease significantly until a shear rate of about $\gamma = 2$. It thus seems at least plausible (but more evidence is required) that the attractor for small (but nonzero) shear rates is space filling. At much larger shear rates there are stable periodic orbits, but it not known whether mesoscopically irreversible attractors with fractal support similar to those in the Lorentz gas exist.

For systems with larger numbers of particles, it becomes totally impractical to calculate the box dimension of the attractor, due to the dimensionality of phase space. However, the other techniques used in this paper, that is, Lyapunov exponents and in particular symbolic dynamics, are both very much applicable to larger systems and we would recommend their use.

Another approach would be to study toy models that are analytically tractable in the hope that features of the transitions in these models are similar to those in more intrinsically interesting systems. In this regard we note that very recently two-dimensional time-reversible dissipative piece-

wise linear maps have been constructed that appear to lead to space-filling attractors [14].

If this type of crisis is generic to many nonequilibrium systems, it would signal the existence of phases that are quite different to those near equilibrium. The macroscopic signa-ture of the mesoscopically irreversible phase would be (Sec. III) the absence of fluctuations in only some components of the dissipative flux, which is the generalization of the cur-rent. There is much to be discovered about steady states far from equilibrium.

---

[1] W. G. Hoover and B. Moran, Phys. Rev. A **40**, 5319 (1989).

[2] G. P. Morriss, Phys. Lett. A **134**, 307 (1989).

[3] W. G. Hoover and H. A. Posch, Phys. Lett. A **123**, 227 (1987).

[4] W. N. Vance, Phys. Rev. Lett. **69**, 1356 (1992).

[5] J. Lloyd, M. Niemeyer, L. Rondoni, and G. P. Morriss, Chaos **5**, 536 (1995).

[6] N. I. Chernov, G. L. Eyink, J. L. Lebowitz, and Ya. G. Sinai, Commun. Math. Phys. **154**, 569 (1993).

[7] D. J. Evans and G. P. Morriss, *Statistical Mechanics of Non-equilibrium Liquids* (Academic, London, 1990).

[8] N. I. Chernov and J. L. Lebowitz, Phys. Rev. Lett. **75**, 2831 (1995).

[9] C. P. Dettmann, G. P. Morriss, and L. Rondoni, Chaos Solitons Fractals (to be published).

[10] J. Lloyd, L. Rondoni, and G. P. Morriss, Phys. Rev. E **50**, 3416 (1994).

[11] I. Procaccia, Phys. Scr. **T9**, 40 (1985).

[12] K. Falconer, *Fractal Geometry and its Applications* (Wiley, Chichester, 1990).

[13] E. Ott, *Chaos in Dynamical Systems* (Cambridge University Press, Cambridge, 1993).

[14] W. G. Hoover, O. Kum, and H. A. Posch, Phys. Rev. E **53**, 2123 (1996).